China Ocean Eng., 2018, Vol. 32, No. 3, P. 365–373
DOI: https://doi.org/10.1007/s13344-018-0038-5, ISSN 0890-5487
http://www.chinaoceanengin.cn/ E-mail: coe@nhri.cn

Experimental Research on Boundary Shear Stress in Typical Meandering Channel

CHEN Kai-hua[a, b, c, d, *], XIA Yun-feng[a, c, d], ZHANG Shi-zhao[a, c, d], WEN Yun-cheng[a, c, d], XU Hua[a, c, d]

[a]Nanjing Hydraulic Research Institute, Nanjing 210029, China

[b]College of Harbor, Coastal and Offshore Engineering, Hohai University, Nanjing 210098, China

[c]The State Key Laboratory of Hydrology-Water Resources and Hydraulic Engineering, Nanjing 210098, China

[d]Key Laboratory of Port, Waterway and Sedimentation Engineering of Ministry of Transport, Nanjing 210024, China

Received January 12, 2018; revised March 19, 2018; accepted April 27, 2018

Abstract

A novel instrument named Micro-Electro-Mechanical System (MEMS) flexible hot-film shear stress sensor was used to study the boundary shear stress distribution in the generalized natural meandering open channel, and the mean sidewall shear stress distribution along the meandering channel, and the lateral boundary shear stress distribution in the typical cross-section of the meandering channel was analysed. Based on the measurement of the boundary shear stress, a semi-empirical semi-theoretical computing approach of the boundary shear stress was derived including the effects of the secondary flow, sidewall roughness factor, eddy viscosity and the additional Reynolds stress, and more importantly, for the first time, it combined the effects of the cross-section central angle and the Reynolds number into the expressions. Afterwards, a comparison between the previous research and this study was developed. Following the result, we found that the semi-empirical semi-theoretical boundary shear stress distribution algorithm can predict the boundary shear stress distribution precisely. Finally, a single factor analysis was conducted on the relationship between the average sidewall shear stress on the convex and concave bank and the flow rate, water depth, slope ratio, or the cross-section central angle of the open channel bend. The functional relationship with each of the above factors was established, and then the distance from the location of the extreme sidewall shear stress to the bottom of the open channel was deduced based on the statistical theory.

Key words: boundary shear stress, flume physical model, river bend, MEMS flexible hot-film shear stress sensor

Citation: Chen, K. H., Xia, Y. F., Zhang, S. Z., Wen, Y. C., Xu, H., 2018. Experimental research on boundary shear stress in typical meandering channel. China Ocean Eng., 32(3): 365–373, doi: https://doi.org/10.1007/s13344-018-0038-5

1 Introduction

This study focuses on the distribution pattern of the boundary shear stress in open channel bend. Early investigations on the boundary shear stress distribution in river bend have been carried out by Johnston (1960), Wright and Carstens (1970), Myers (1978), Rajaratnam and Rai (1979), Whiting and Dietrich (1990) and Shiono and Knight (1991). These early researches mainly focused on straight open channels with gentle slope banks. Johnston (1960) presented the methods for treating a turbulent three-dimensional boundary layer at a symmetric plane, and a reasonable agreement with the experiment was achieved by the use of the momentum integral techniques in the prediction of the momentum thickness, shape factor, boundary shear stress, and the location of separation zone. Shiono and Knight (1991) derived the theoretical expression of the lateral distributions of the depth-average velocity and boundary shear stress for channels of any shape, provided that the boundary geometry can be discretized into the linear elements. The analytical model which derived by Shiono and Knight (1991) includes the effects of the bed-generated turbulence, lateral shear turbulence and secondary flows. Experimental data from the Science and Engineering Research Council (SERC) Flood Channel Facility are used to illustrate the relative importance of these three effects on internal shear stresses. In the last decade, several studies have been reported by Guo and Julien (2005), Yang et al. (2012), Kean et al. (2009), Ansari et al. (2011), Kabiri-Samani et al. (2013), Kordi et al. (2015), Tang and Knight (2009), Xiao et al. (2016), Khozani et al. (2017), Devi and Khatua (2017) and Xiang et al. (2017). Guo and Julien (2005) proposed an analytical solution to predict the mean riverbed, and sidewall

Foundation item: This work is financially supported by the National Key R&D Program of China (Grant No. 2016YFC0402306) and the National Natural Science Foundation of China (Grant No. 51779149).

*Corresponding author. E-mail: 415304706@qq.com

shear stress in straight rectangular open channel flows without taking the secondary flow and bed and bank roughness into account. Yang et al. (2012) presented an approach for predicting the velocity distribution and boundary shear stress by applying the Reynolds equations. Kordi et al. (2015) performed a modified Shiono and Knight (1991) method which is suitable for various kinds of the boundary conditions including laboratory and natural conditions. Concerning the physical model, Kean et al. (2009) presented high-precision measurements of the boundary shear stress across the straight channel and evaluated the interaction between the width-to-depth ratio and the distribution law of the boundary shear stress. Nortek ADV was implemented by Xiang et al. (2017) to study the boundary shear stress pattern in a sharp open channel bend while the relationship between the boundary shear stress and the flow parameters or the section shapes was not studied in the research of Xiang et al. (2017). The University of Birmingham, UK has carried out the classical Flood Channel Facility (FCF) series physical experiments during the years from 1980 to 1997 using the LDA laser Doppler technology to study the boundary shear stress of a simple trapezoidal open channel or a compound open channel and the lateral distribution of the boundary shear stress in the straight open channel was analyzed. However, the distribution pattern of the average sidewall shear stress along the open channel was not discussed throughout the FCF study. The FCF series experiments mainly focused on the boundary shear stress pattern in the simple open channel and compound open channel and ignore the case of generalized natural open channel bend. The boundary shear stress pattern obtained in the FCF experiments was based on the flow measurements, and there existed inescapable experimental errors in the calculation process from the velocity to obtain the boundary shear stress (Knight and Sellin, 1987).

To sum up, the previous studies have not systematically analyzed the average sidewall shear stress distribution along the concave and convex bank and the lateral distribution of the boundary shear stress in the generalized natural open channel bend. To enrich this research field, the Micro-Electro-Mechanical System (MEMS) flexible hot-film shear stress sensor was used to study the boundary shear stress distribution in the generalized natural meandering open channel and the sidewall shear stress distribution along the meandering channel and the lateral boundary shear stress distribution in the typical cross-section. Based on the measurement of the boundary shear stress, a semi-empirical semi-theoretical boundary shear stress algorithm was derived, and a comparison between previous research and this study had been made. Finally, a single factor analysis was made on the relationship between the average sidewall shear stress on the convex and concave bank and the flow rate, water depth, slope ratio, or the cross-section central angle of the open channel bend. The functional relationship with each of the above factor was established, and the distance from the location of the extreme sidewall shear stress to the bottom of the open channel is thus deduced based on the statistical theory.

2 Experimental methodology and measurement

The river bend channel used has the dimensions of 38 m in length, 3.5 m in width and 0.8 m in depth and the channel bed and walls are made of concrete. The main bend channel consisted of the measuring weir, feeder canal, experimental sections, settling tank and backwater channel. The physical experiment is controlled by a steady flow. The upstream inlet is connected to the measuring weir, the butterfly valve used to control the downstream water level, and 14 water level observation points set for real-time monitoring. The length of the straight transition section between the upper and lower open channel bend is 3–5 times the width of the flume to ensure the uniformity of the flow in the bend and to ensure that the secondary flow is sufficiently attenuated in the downstream of the open channel bend.

As shown in Fig. 1, the generalized natural meandering channel is divided into 12 sections to measure the boundary shear stress. Cross-sections #0 and #11 are in the form of isosceles trapezoid, and the generalization of Cross-sections #1–#10 is based on the research of Wang et al. (2005). According to the relevant researches, the entrance of the open channel bend can be generalized to a U-shaped cross-section and the cross-section in the open channel bend can be generalized into a symmetrical or asymmetrical V-shaped cross-section. The deep groove is inclined toward the concave bank, and the downstream of the open channel bend can be generalized to a U-shaped cross-section (Wang et al., 2005). The dashed line in Fig. 1 refers to the envelope of the deep groove area and the open area of every cross-section is strictly identical when generalizing the cross-sections of this open channel bend flume. In this study, the concept of the cross-section central angle is defined. In Fig. 1, the cross-section central angle of Section #0 is defined as –10°, one of Section #1 is 0° and so on. Therefore, the central angle of Section #11 is 100°.

The experimental conditions of the river bend are shown in Table 1. The design of experimental conditions compre-

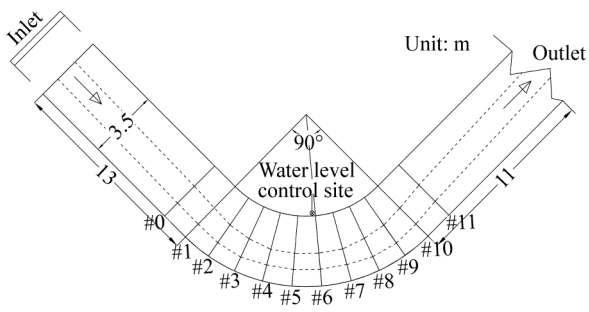

Fig. 1. Plan view of the river bend in an open channel flume.

Table 1 Epitome of the river bend experimental conditions

Test case	Q (m^3/s)	H (m)	V (m/s)	Re ($\times10^5$)	Slope ratio	Fr ($\times10^{-4}$)
1	0.0435	0.20	0.15	57	1:1.5	0.6036
2	0.0820	0.25	0.20	76	1:1.5	1.0730
3	0.1388	0.30	0.25	95	1:1.5	1.6766
4	0.1619	0.35	0.25	95	1:1.5	1.6766
5	0.2220	0.40	0.30	114	1:1.5	2.4143
6	0.2318	0.45	0.25	95	1:1.5	1.6766
7	0.0435	0.20	0.15	57	1:2.0	0.6036
8	0.0820	0.25	0.20	76	1:2.0	1.0730
9	0.1388	0.30	0.25	95	1:2.0	1.6766
10	0.1619	0.35	0.25	95	1:2.0	1.6766
11	0.2220	0.40	0.30	114	1:2.0	2.4143
12	0.2318	0.45	0.25	95	1:2.0	1.6766
13	0.0435	0.20	0.15	57	1:2.5	0.6036
14	0.0820	0.25	0.20	76	1:2.5	1.0730
15	0.1388	0.30	0.25	95	1:2.5	1.6766
16	0.1619	0.35	0.25	95	1:2.5	1.6766
17	0.2220	0.40	0.30	114	1:2.5	2.4143
18	0.2318	0.45	0.25	95	1:2.5	1.6766

hensively takes the influence of velocity, water depth, and the slope ratio on the pattern of the boundary shear stress into account. The bank toe is regarded as a reference point throughout the experiments. The Micro-Electro-Mechanical System (MEMS) flexible hot-film shear stress sensor is set every 5–10 cm in the perimeter of the cross-section, and both ten boundary shear stress measured points are arranged on the cross-sections of the concave and convex bank, and 6–8 boundary shear stress measured points are set on the open channel bed.

The overall test conditions are given in Table 1 where Q is the inlet flow rate, H is the water depth at the slope, V is the water velocity, Re is the Reynolds number, s is the slope ratio of the channel (1: s=vertical : horizontal) and Fr is the Froude number. In the experiment, the boundary shear stress was measured by Micro-Electro-Mechanical System (MEMS) flexible hot-film shear stress sensor (Xu et al., 2015; Hao et al., 2017).

3 Experimental results

3.1 Sidewall shear stress distribution along the open channel bend

In this study, we studied the distribution of average sidewall shear stress along the open channel bend in the concave and convex banks and the cross-section distribution of the boundary shear stress through the accurate measurement in the generalized natural open channel bend. The calculation of the average sidewall shear stress of the concave and convex banks is based on the integral of measured data for the concave and convex banks of the open channel bend. The distribution of the average sidewall shear stress (τ_w) distribution along the open channel bend was analyzed. As shown in Fig. 2, the graph reveals the variation tendency of the average sidewall shear stress distribution in the concave bank with the cross-section central angle (θ) under three different bank slope ratios (s).

From Fig. 2, we can conclude that the average sidewall shear stress distribution is apparently different with different cross-section central angles. It appears to be a semi-bimodal distribution of the average sidewall shear stress in the concave bank of the open channel bend from the entrance cross-section to the exit cross-section.The average sidewall shear stress at the entrance section of the open channel bend is relatively low, and it gradually rises in the open channel bend and reaches the extreme value in the downstream cross-section of the apex of the open channel bend. This phenomenon is closely related to the turbulence of the secondary flow near the concave side of the bank.

As shown in Fig. 3, the pattern of the sidewall shear stress distribution in the toe of the concave bank shows a bimodal shape along the river bend. After the water flows into the bend, the sidewall shear stress in the toe of the concave bank begins to rise and reaches the extreme value in the downstream of the river bend apex.

As can be seen from Fig. 4, the average sidewall shear stress distribution along the convex bank is inconsistent with that along the concave bank, while both appear to be semi-bimodal shape and the locations of the extreme sidewall shear stress value are entirely different. The extreme value of the average sidewall shear stress in the convex bank appears in the downstream of the bend entrance and the outlet of the river bend. The minimal value of the average sidewall shear stress in the convex bank exists in the apex of the river bend. As the water flows into the bend, the main current gradually deflects towards the concave bank, and the turbulence on the convex bank side is weak. According to the measured value, the value of the average shear stress on the convex bank is about 70% of that on the

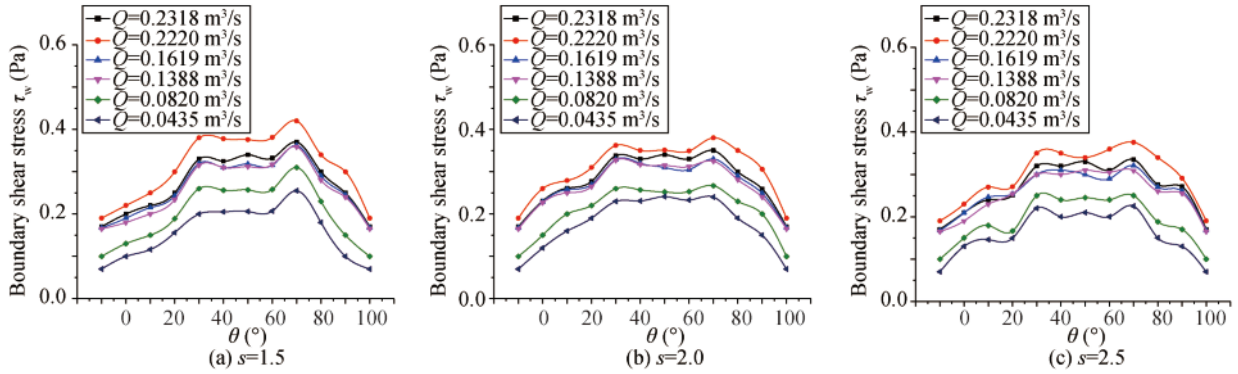

Fig. 2. Average boundary shear stress distribution in the concave bank vs. the cross-section central angle.

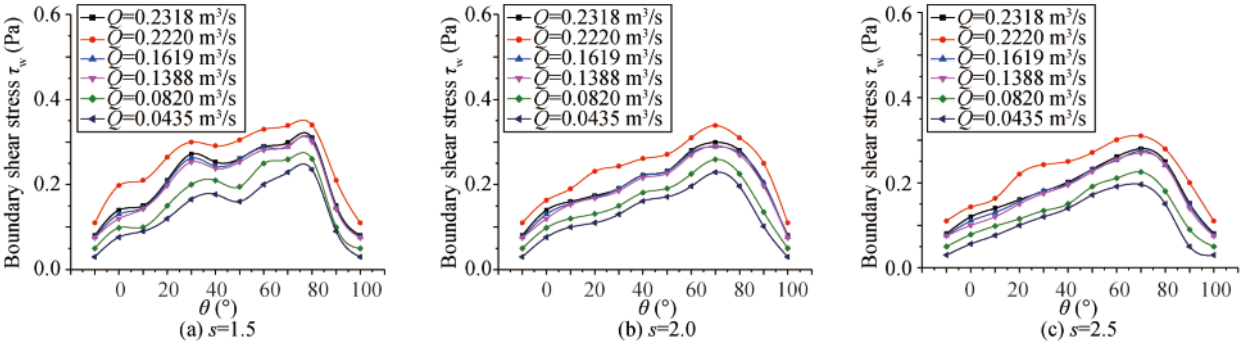

Fig. 3. Boundary shear stress distribution in the toe of the concave bank vs. the cross-section central angle.

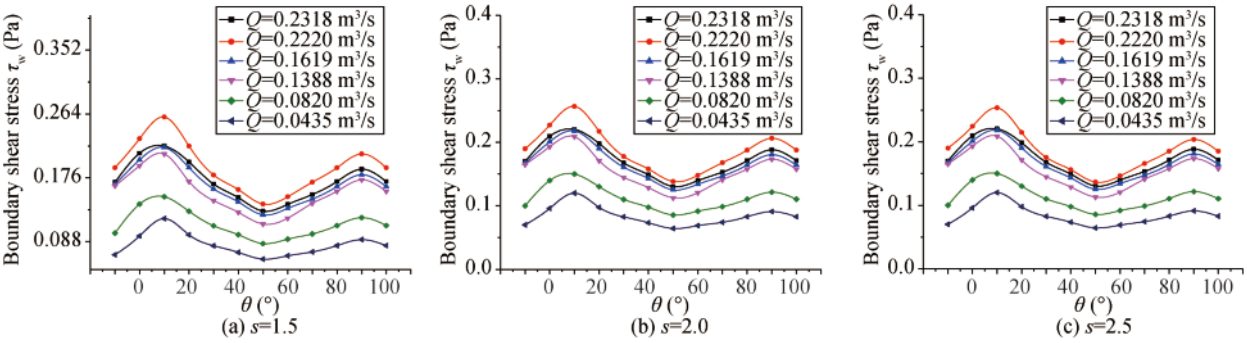

Fig. 4. Average boundary shear stress distribution in the convex bank vs. the cross-section central angle.

concave bank. After flowing the apex of the river bend, the main current begins to move to the center line of the open channel bend. The value of the average shear stress in the convex bank gradually increases. The pattern of the average sidewall shear stress distribution along the open channel bend confirms the scour and deposition characteristics of the natural meandering channel. The relatively low sidewall shear stress in the convex bank triggers the sand deposition in the convex bank while the concave bank experiences severe scour due to high sidewall shear stress.

As can be seen from Fig. 5, the sidewall shear stress distribution in the toe of the convex bank of the open channel bend along the flume shows a bimodal pattern. The extreme value appears to exist in the downstream of the apex cross-section and the outlet of the river bend. This distribution pattern is directly related to the deflection of the main current and the shape of the generalized natural open channel bend.

3.2 Lateral distribution of the boundary shear stress

Yuen (1989) have studied the lateral distribution pattern of the boundary shear stress on the straight open channel. Our study conducted a detailed measurement of the boundary shear stress of the typical cross-section in the lateral direction of the generalized natural river bend. A comparison between the research of Yuen (1989) and our study has been made. The lateral distribution pattern of the boundary shear stress in generalized natural open channel bend is shown in

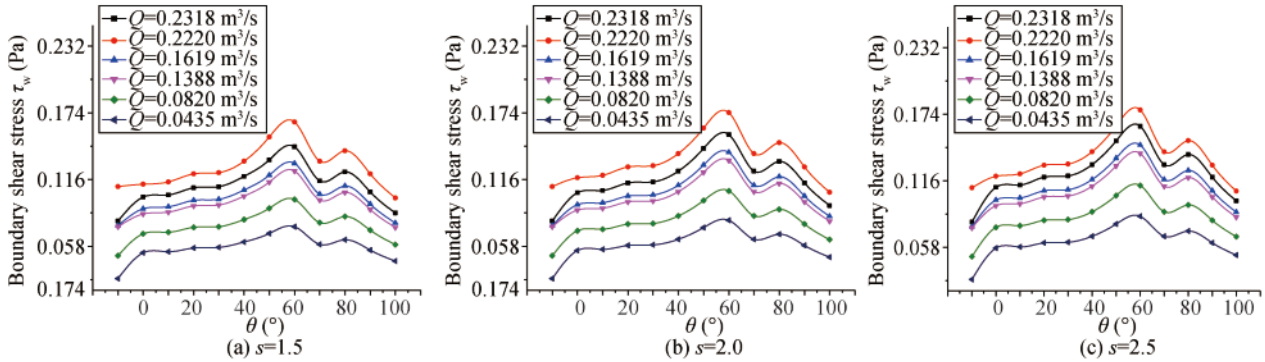

Fig. 5. Boundary shear stress distribution in the toe of the convex bank of the open channel bend vs. the cross-section central angle.

Fig. 6. According to the research of Yuen (1989), the lateral distribution of the boundary shear stress in the typical cross-section of the straight channel shows a symmetric pattern and the extremum of the boundary shear stress is located near the center point of the river bed. In our study, a different lateral distribution pattern has been found. In the transition part of the river bend which belongs to the straight open channel, the lateral distribution of the boundary shear stress shares the same pattern with the study of Yuen (1989). However, the lateral distribution of the boundary shear stress in the river bend is obviously asymmetric. It varies with the main current deflection and the section morphology. According to Fig. 7, the extremum of the lateral boundary shear stress is located on the concave bank, and the distance between the river bed to the place of the extreme boundary shear stress is almost the same. Due to the fact that the research on the lateral distribution of boundary shear stress in the generalized natural river bend has not been systematically carried out previously, the measurement results of the lateral boundary shear stress distribution in this study can provide a reference for future numerical model calculations.

From Fig. 6 and Fig. 7, it can be seen in the straight transition section of the open channel bend which is an isosceles trapezoidal cross-section and the boundary shear stress shows a symmetrical distribution pattern. The boundary shear stress in the convex bank increases first from the toe and decreases to the minimum value near the surface. The distribution pattern of the boundary shear stress shows the regular phenomenon of double-peaks and double-val-

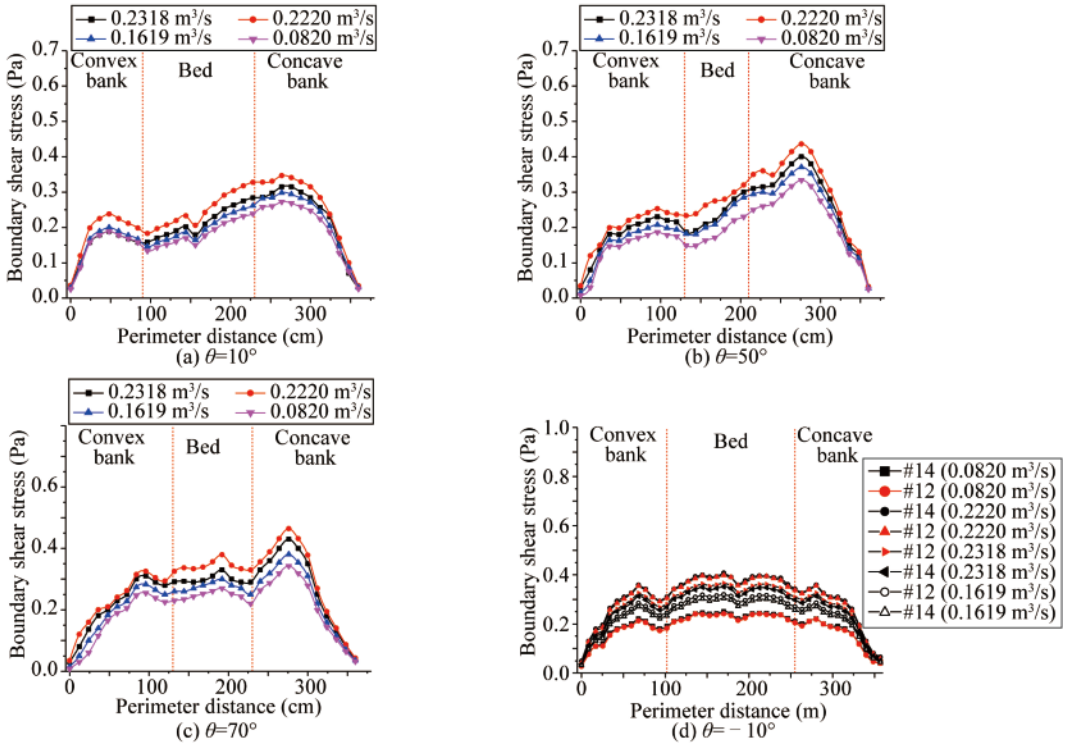

Fig. 6. Lateral distribution of the boundary shear stress in the typical cross-section.

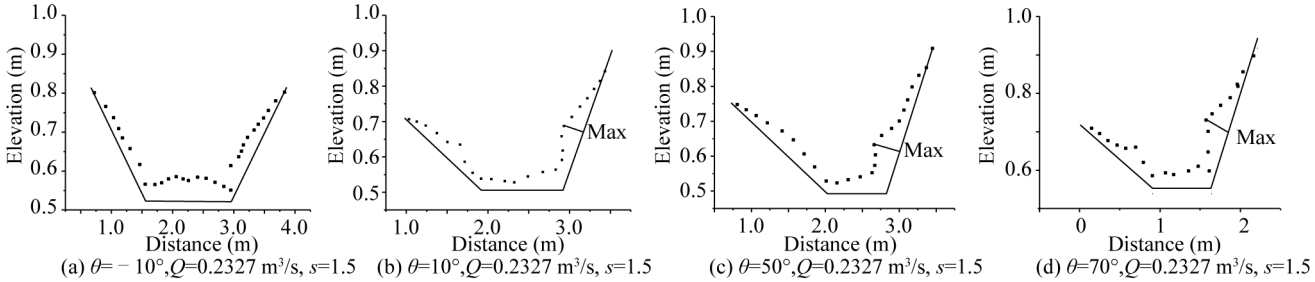

(a) θ= − 10°,Q=0.2327 m³/s, s=1.5 (b) θ=10°,Q=0.2327 m³/s, s=1.5 (c) θ=50°,Q=0.2327 m³/s, s=1.5 (d) θ=70°,Q=0.2327 m³/s, s=1.5

Fig. 7. Lateral distribution of the boundary shear stress in the typical cross-section with the extreme value depicted.

leys trend. The distribution pattern of the boundary shear stress in the concave bank is similar to that of the convex bank. The results of this study on the distribution pattern of the boundary shear stress at the transitional cross-section of the straight channel are similar to those of Yuen (1989).

After the flow enters the bend, the slope of the concave bank becomes steeper and the main current starts to deflect to the concave bank while the shape of the open channel cross-section gradually changes from U-shaped to V-shaped. The above phenomenon leads to the gradual increase of the boundary shear stress on the concave bank. Thus, the boundary shear stress on the concave bank is 20%–30% larger than that of the convex bank.

The boundary shear stress on the concave bank is significantly greater than that of the convex bank when the cross-section central angle is 10°, and there is the minimum value near the center of the bed. In the apex cross-section, the cross-section is V-shaped, and the boundary shear stress of the convex bank is apparently weaker than that of the concave bank while the thalweg and main current deflect to the concave bank.

Boundary shear stress appears to increase first and then decrease from the toe to the water surface in the convex bank. The boundary shear stress near the concave bank is apparently larger than that of the convex bank. The boundary shear stress on the concave bank is approximately 1.24–1.37 times that of the convex bank.

In the downstream of the open channel bend, the boundary shear stress in the downstream section is larger than that in the apex section while the momentum exchange in the boundary layer of the concave bank is enhanced due to the water jacking and the main current deflection. With the gradual change of the cross-section shape from V-shaped to the U-shaped, the thalweg begins to return to the centerline of the bend, and the difference of the boundary shear stress between the convex bank and concave bank decreases. The distribution pattern experiences a similar manner with that of the apex cross-section of the bend.

4 Derivation and discussion

4.1 Derivation of the boundary shear stress algorithm

Based on the above measured results in the generalized open channel bend, combining with the theoretical derivation and the data fitting, a semi-experiential and semi-theoretical boundary shear stress algorithm is proposed.

The semi-experiential and semi-theoretical boundary shear stress algorithm is based on the SKM algorithm first proposed by Shiono and Knight (1991). The expression of the SKM method is:

$$\rho g H S_0 + \left[\frac{\partial H\left(\overline{\tau_{yx}}\right)}{\partial y}\right] - \tau_b \sqrt{1+s^{-2}} = \rho\left[\frac{\partial H(\overline{uv})_d}{\partial y}\right] + 2\rho\int_0^H\left(\frac{\overline{uv}}{2r}+\frac{\overline{u'v'}}{r}\right)dz. \quad (1)$$

Eq. (1) is the simplified form of the SKM model, in which S_0 is the channel bed slope; r is the radius of the curvature; τ_b is the local boundary shear stress; ρ is the fluid density; g is the gravitational acceleration; x, y, and z are the streamwise, lateral and vertical coordinates, respectively; u, v, and w are the velocity components in the x, y, and z directions, respectively; $\bar{u}$, $\bar{v}$, and $\bar{w}$ are the components of the time-averaged velocities; u', v', and w' are the fluctuation velocity components; $\rho[\partial H(\overline{uv})_d/\partial y]$ refers to the secondary flow term; $\rho\int_0^H\left(\frac{\overline{uv}}{2r}+\frac{\overline{u'v'}}{r}\right)dz$ refers to the curvature-induced additional Reynolds stress. Here, we adopt the hypothesis raised by Knight et al. (2007) and Devi and Khatua (2017), then Eq. (2) and Eq. (3) are obtained:

$$\rho\left[\frac{\partial H(\overline{uv})_d}{\partial y}\right] + 2\rho\int_0^H\left(\frac{\overline{uv}}{2r}+\frac{\overline{u'v'}}{r}\right)dz=\rho g H S_0(1-k)+ny; \quad (2)$$

$$k = F(\theta, Re), \quad (3)$$

where n is a constant which can be determined by the measured data, and k is the function of the cross-section central angle and the Reynolds number. From the results of the above experiments, we can see that the boundary shear stress of each cross-section in the open channel bend is not the same, and the wall shear stress is closely related to the secondary flow. Thus, supposing that the k-factor is a function of the cross-section central angle and the Reynolds number, this assumption includes the consideration of the curvature of the meandering channel.

then Eq. (4) can be obtained:

$$\rho gHS_0+\left[\frac{\partial H\left(\overline{\tau_{yx}}\right)}{\partial y}\right]-\tau_b\sqrt{1+s^{-2}}=\rho gHS_0(1-k)+ny. \quad (4)$$

By assuming that $\tau_b=\left(\frac{f_b}{8}\right)\rho U_d^2$, $\overline{\tau_{yx}}=\rho\lambda U_* H\frac{\partial U_d}{\partial y}$, $U_*=(\tau_b/\rho)^{\frac{1}{2}}$, the final expression is obtained as:

$$\rho gHS_0-\left(\frac{f_b}{8}\right)\rho U_d^2\left(\sqrt{1+s^{-2}}\right)+\frac{\partial}{\partial y}\left[\rho\lambda H^2\left(\frac{f_b}{8}\right)^{\frac{1}{2}}U_d\frac{\partial U_d}{\partial y}\right]=\rho gHS_0(1-k)+ny, \quad (5)$$

where f_b is the Darcy-Weisbach friction factor; λ denotes the dimensionless eddy viscosity, and for the trapezoidal open channel bend, λ=0.16; U_* is the shear velocity; U_d indicates the depth-averaged velocity.

By solving Eq. (5), the final expression of the boundary shear stress is:

$$\tau_b=\frac{f_b}{8}\rho\left[A_3\left(H+\frac{y}{s}\right)^{\alpha}+A_4\left(H+\frac{y}{s}\right)^{-(\alpha+1)}+\omega\left(H+\frac{y}{s}\right)+\eta\right];$$

$$\alpha=-0.5+0.5\sqrt{1+\frac{s\sqrt{1+s^2}}{0.07}\sqrt{8f_b}};$$

$$\omega=\frac{gS_0-ns/\rho}{\frac{\sqrt{1+s^2}}{s}\frac{f_b}{8}-\frac{\lambda}{s^2}\sqrt{\frac{f_b}{8}}};$$

$$\eta=\frac{\rho gHS_0(k-1)+nHs}{\rho\sqrt{1+s^{-2}}\frac{f_b}{8}}, \quad (6)$$

where A_3 and A_4 are constants.

Due to the undetermined parameters in Eq. (6), the final expression is obtained as Eq. (7), which is a semi-empirical and semi-theoretical expression of the boundary shear stress in the generalized natural open channel bend according to the experimental data of the boundary shear stress measured experiment.

$$\tau_b=\frac{f_b}{8}\rho\left[2.22\left(H+\frac{y}{s}\right)^{\alpha}-3.52\times10^{-4}\left(H+\frac{y}{s}\right)^{-(\alpha+1)}+\omega\left(H+\frac{y}{s}\right)+\eta\right];$$

$$\alpha=-0.5+0.5\sqrt{1+\frac{s\sqrt{1+s^2}}{0.07}\sqrt{8f_b}};$$

$$\omega=\frac{gS_0-17.5s}{\frac{\sqrt{1+s^2}}{s}\left(\frac{f_b}{8}\right)-\frac{0.07}{s^2}\sqrt{\frac{f_b}{8}}};$$

$$\eta=\frac{\rho gHS_0(k-1)+17.5Hs}{1000\sqrt{1+s^{-2}}\frac{f_b}{8}};$$

$$k=1.384(\sin\theta)^{28.28}+0.096\ln Re, R^2=0.91. \quad (7)$$

The comparison was made between the semi-experiential and semi-theoretical boundary shear stress model of this study and those in the previous research, i.e., the approximations of the expression derived by Devi and Khatua (2017) and Kordi et al. (2015).

According to Fig. 8, the difference between the calculated value of the boundary shear stress by the semi-empirical formula put forward by this study and the measured value is about 4% to 7% which shows a slight improvement over the methods derived by the previous researches. In the previous researches, the formulas of Devi and Khatua (2017) and Kordi et al. (2015) are better than that of Yang et al. (2012) in accuracy and the error is between 5% and 9% while the error of Yang et al.'s formula is between 10% and 20%. Both the formulas of Devi and Khatua (2017) and Kordi et al. (2015) considered the secondary flow and Reynolds number of the bend on the basis of the Shiono and Knight (1991) method without considering the influence of the central angle on the wall shear stress. Since the formulas of Devi and Khatua (2017) and Kordi et al. (2015) ignored the differences between the lateral distributions of the boundary shear stress in the river bend section, and only the effects of the Reynolds number and secondary flow were considered. Therefore, a non-negligible difference between the measured and calculated results existed. While in this study, a detailed measurement of the boundary shear stress was conducted in order to study the distribution of the boundary shear stress in the meandering channel, and from the experimental results we can see that the consideration of the central angle is really necessary.

4.2 Discussion on the sidewall shear stress distribution pattern in the generalized natural open channel bend

In this paper, single factor analysis of the relationship between the average sidewall shear stress on the concave and convex banks and the discharge, water depth, slope ratio, and cross-section central angle was made. The results are shown in Fig. 9 and Fig. 10. As shown in Fig. 9, the relationship between the average sidewall shear stress of the concave bank and the cross-section central angle shows a unimodal function trend and the peak appears at the apex section. The average sidewall shear stress on the concave

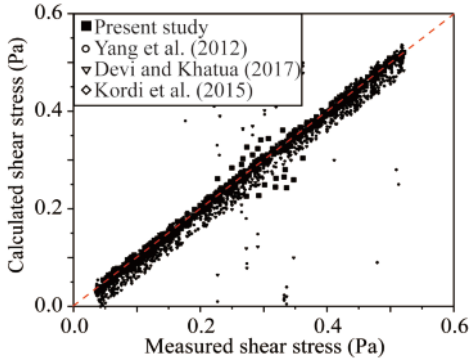

Fig. 8. All experimentally measured shear stress data (over 3000 measured data) along the wetted perimeter of the river bend bank slope compared with the results from Yang et al. (2012), Devi and Khatua (2017) and Kordi et al. (2015).

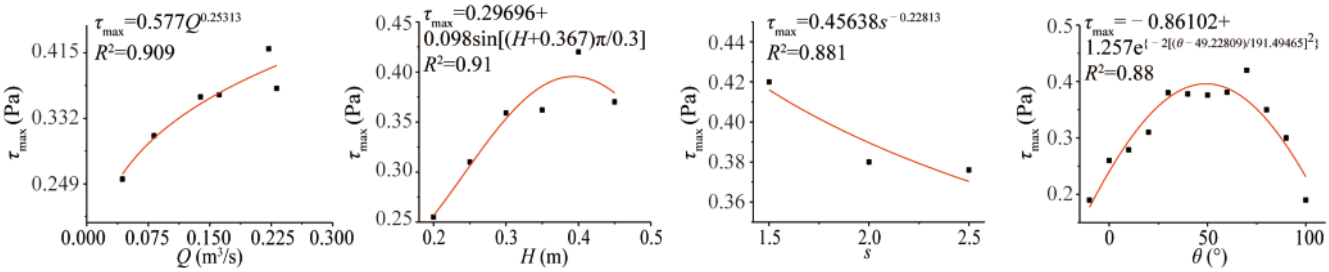

Fig. 9. Relationships between the average boundary shear stress in the concave bank and the discharge, water depth, slope ratio andcross-section central angle.

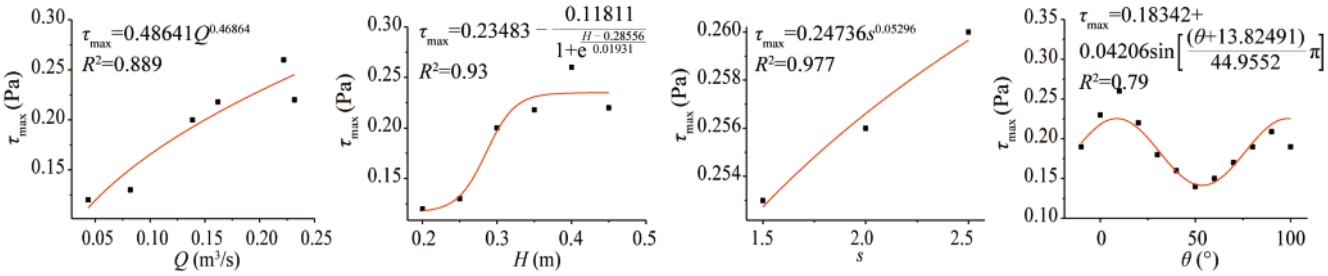

Fig. 10. Relationships between the average boundary shear stress in the convex bank and the discharge, water depth, slope ratio and cross-section central angle.

bank increases with the increase of the incoming flow discharge, and there is a clear positive correlation between the discharge and average sidewall shear stress on the concave bank. When the water depth is smaller than 35 cm, the average sidewall shear stress of the concave bank is positively correlated with the water depth. Whereas, when the water depth is larger than 35 cm, it is negatively correlated with the water depth. The average sidewall shear stress of the concave bank decreases with the increase of the bank slope ratio. The functional relationships between the average sidewall shear stress and the discharge, water depth, bank slope ratio, cross-section central angle are predicted, and the fitting relationship can be used in the prediction and analysis of the average sidewall shear stress of the concave bank in the generalized open channel bend.

The same analysis is made in the average sidewall shear stress of the convex bank. As shown in Fig. 10, the average sidewall shear stress on the convex bank increases with the increase of the bank slope ratio, water depth, and flow discharge. However, it reaches the minimum value at the apex cross-section in the open channel bend. Whereas, the maximum value is achieved at the entrance of the open channel bend.

To sum up the above analysis, it can be concluded that the average sidewall shear stress of the generalized open channel bend varies with the flow discharge, water depth, bank slope ratio, and cross-section central angle. The reason for the difference is that the sidewall shear stress of both convex bank and concave bank is simultaneously affected by the secondary flow and the shape of the cross-section. The combined effects of the main current deflection and the secondary flow are the key factor to influence the distribution pattern of the sidewall shear stress.

In this study, the expression of the elevation of the extreme value of the sidewall shear stress on the concave bank of the generalized open channel is deduced based on the statistical theory as:

$$h_b = 0.11\bar{p}\sin\left(\arctan\frac{1}{s}\right), \tag{8}$$

where h_b refers to the elevation of the extreme value of the sidewall shear stress on the concave bank of the generalized open channel, and $\bar{p}$ refers to the wetted perimeter of the concave bank.

5 Conclusions

In this study, a novel instrument named Micro-Electro-Mechanical System (MEMS) flexible hot-film shear stress sensor was used to conduct a boundary shear stress measurement experiments in the generalized natural open channel bend. The distribution pattern along the open channel bend and the lateral distribution pattern of the boundary shear stress in the bend were analyzed in detail. Meanwhile, a formula for the boundary shear stress computation on the generalized natural open channel bend was derived based on the classical N-S equations, and the comparison between the previous studies and this study had been implemented. According to the comparison, the formula obtained in this study has reached a better accuracy. The boundary shear stress formula derived in this study is based on the classical SKM model, and comprehensive consideration of such

factors as the cross-section central angle and the Reynolds number. In the meantime, the measured data in the experiments were used to calibrate the formula, which better represented the characterization of the boundary shear stress distribution. Finally, single factor analysis is made on the relationships between the average sidewall shear stress and the discharge, water depth, bank slope ratio and cross-section central angle. Based on the analysis, it is found that the average sidewall shear stress of the concave bank is positively correlated with the flow discharge and water depth. However, the bank slope ratio is negatively correlated, and the maximum average sidewall shear stress is found in the apex cross-section. The average sidewall shear stress of the convex bank is positively associated with the bank slope ratio, water depth and flow discharge and the minimum value of the average sidewall shear stress are near the apex cross-section. Based on the general theory of statistics, the expression of the elevation of the maximum sidewall shear stress is derived in the end.

References

Ansari, K., Morvan, H.P. and Hargreaves, D.M., 2011. Numerical investigation into secondary currents and wall shear in trapezoidal channels, *Journal of Hydraulic Engineering*, 137(4), 432–440.

Devi, K. and Khatua, K.K., 2017. Depth-averaged velocity and boundary shear stress prediction in asymmetric compound channels, *Arabian Journal for Science and Engineering*, 42(9), 3849–3862.

Guo, J.K. and Julien, P.Y., 2005. Shear stress in smooth rectangular open-channel flows, *Journal of Hydraulic Engineering*, 131(1), 30–37.

Hao, S.Y., Xia, Y.F. and Xu, H., 2017. Experimental study on the bed shear stress under breaking waves, *China Ocean Engineering*, 31(3), 308–316.

Johnston, J.P., 1960. The turbulent boundary layer at a plane of symmetry in a three-dimensional flow, *Journal of Basic Engineering*, 82(3), 622–628.

Kabiri-Samani, A., Farshi, F. and Chamani, M.R., 2013. Boundary shear stress in smooth trapezoidal open channel flows, *Journal of Hydraulic Engineering*, 139(2), 205–212.

Kean, J.W., Kuhnle, R.A., Smith, J.D., Alonso, C.V. and Langendoen, E.J., 2009. Test of a method to calculate near-bank velocity and boundary shear stress, *Journal of Hydraulic Engineering*, 135(7), 588–601.

Khozani, Z.S., Bonakdari, H. and Zaji, A.H., 2017. Estimating the shear stress distribution in circular channels based on the randomized neural network technique, *Applied Soft Computing*, 58(3), 441–448.

Knight, D.W. and Sellin, R.H.J., 1987. The SERC flood channel facility, *Water and Environment Journal*, 1(2), 198–204.

Knight, D.W., Omran, M. and Tang, X.N., 2007. Modeling depth-averaged velocity and boundary shear in trapezoidal channels with secondary flows, *Journal of Hydraulic Engineering*, 133(1), 39–47.

Kordi, H., Amini, R., Zahiri, A. and Kordi, E., 2015. Improved Shiono and Knight method for overflow modeling, *Journal of Hydrologic Engineering*, 20(12), 1–10.

Myers, W.R.C., 1978. Momentum transfer in a compound channel, *Journal of Hydraulic Research*, 16(2), 139–150.

Rajaratnam, N. and Rai, S.P., 1979. Plane turbulent wall wakes, *Journal of the Engineering Mechanics Division*, 105(5), 779–794.

Shiono, K. and Knight, D.W., 1991. Turbulent open-channel flows with variable depth across the channel, *Journal of Fluid Mechanics*, 222, 617–646.

Tang, X.N. and Knight, D.W., 2009. Lateral distributions of streamwise velocity in compound channels with partially vegetated floodplains, *Science in China*, *Series E*: *Technological Sciences*, 52(11), 3357–3362.

Wang, F.X., Guo, Z.M., Wang, L.Q., Lu, J., 2005. The flexural shape characters at middle reaches of Huaihe River, *Journal of Anhui Technical College of Water Resources and Hydroelectric Power*, 5(1), 5–7. (in Chinese)

Whiting, P.J. and Dietrich, W.E., 1990. Boundary shear stress and roughness over mobile alluvial beds, *Journal of Hydraulic Engineering*, 116(12), 1495–1511.

Wright, R.R. and Carstens, M.R., 1970. Linear-momentum flux to overbank sections, *Journal of the Hydraulics Division*, 96(9), 1781–1793.

Xiang, Y., Yu, M.H., Wei, H.Y. and Yu, F., 2017. Calculation method of boundary shear stress in a sharply-curved channel, *Advanced Engineering Sciences*, 49(2), 45–53. (in Chinese)

Xiao, Y., Zhou, G., and Yang, F.S., 2016. 2D numerical modelling of meandering channel formation, *Journal of Earth System Science*, 125(2), 251–267.

Xu, H., Xia, Y.F., Ma, B.H., Hao, S.Y., Zhang, S.Z. and Du, D.J., 2015. Research on measurement of bed shear stress under wave-current interaction, *China Ocean Engineering*, 29(4), 589–598.

Yang, S.Q., Dharmasiri, N. and Han, Y., 2012. Momentum balance method and estimation of boundary shear stress distribution, *Journal of Hydraulic Engineering*, 138(7), 657–660.

Yuen, K.W.H., 1989. *A Study of Boundary Shear Stress*, *Flow Resistance and Momentum Transfer in Open Channels with Simple and Trapezoidal Cross Section*, Birminghan University, Birminghan, UK.